

# Mixing Volume Model for Molecular Diffusion and Thermal Conduction in Compressible Turbulence

Y. Tai\*, T. Watanabe\* and K. Nagata\*

Corresponding author: tai.youming@g.mbox.nagoya-u.ac.jp

\* Department of Aerospace Engineering, Nagoya University, Nagoya, Japan.

June 15, 2018

**Abstract:** We study performance of mixing volume model (MVM), which is a model for molecular diffusion and thermal conduction based on interactions among spatially distributed computational particles, in compressible turbulence. *A-priori* test is performed with direct numerical simulation (DNS) database of compressible turbulent planar jets with passive scalar transfer. The results show that the MVM well predicts molecular diffusion and thermal conductive terms, which appear in passive scalar and internal energy transport equations, respectively. It is also shown that the MVM works better when the particle density is high while a higher particle density is required for higher jet Mach number.

*Keywords:* Compressible Turbulence, Molecular Diffusion, Heat Conduction, Mixing Volume Model.

## 1 Introduction

Mixing in compressible turbulence is an important phenomenon in various engineering applications as well as fundamental physics. A turbulent mixing process comprises turbulent diffusion stirring a fluid and molecular diffusion causing mixing at a molecular level. It should be noted that chemical reaction rate in industrial flows, e.g., in a direct injection engine, is often controlled by molecular diffusion, which strongly depends on small scale turbulence. Nowadays, for such complex flows in engineering applications, most computational fluid dynamics (CFD) rely on an approach based on Reynolds-averaged Navier-Stokes equation (RANS, [1]) because of its low computational cost. An alternative numerical approach is Large eddy simulation (LES) [2]. In LES, large scale motions of a turbulent flow are directly computed while effects of small-scale motions need to be modeled by subgrid scale (SGS) models. Hence, LES is more accurate than RANS, which models all the scales that are present in the turbulent flow, though the computational cost of LES is higher than RANS. Because of rapid progress of computational resource, LES has currently become the most viable/promising numerical tool for simulating realistic unsteady turbulent flows.

In LES of a turbulent reacting flow, several subgrid scale (SGS) models have been proposed for closing a chemical source term [3, 4]. However, it is not clear how these SGS models deal with various reaction schemes, where the model might be optimized for a specific chemical reaction. Instead of modeling the SGS effects on the chemical source term, recent LES of reactive flow utilizes Lagrangian notional particles to simulate reactive scalars [5, 6]. However, this approach requires modeling molecular diffusion, where such models are called a mixing model. Various mixing models [7] have been developed for RANS-type simulations. In these models, mixing timescale  $\tau_\phi$  appears as an unknown quantity, and it is often computed with a scalar-to-mechanical time scale ratio  $C_\phi$  defined with Reynolds-averaged quantities. However, the mixing model for the LES needs to compute  $C_\phi$  as a function of space and time, and therefore, a different method to compute the mixing timescale is required in LES. For addressing this issue, mixing volume model (MVM) [8] was developed as a LES-type mixing model. The MVM uses a relaxation process to a low-pass

Table 1: Physical and computational parameters of the DNS.

	Run A	Run B	Run C	Run D
Jet Reynolds number $Re_J$	14000	14000	14000	32000
Jet Mach number $M_J$	0.6	1.6	2.6	1.6
Schmidt number $Sc$	1.0	1.0	1.0	1.0
Prandtl number $Pr$	0.7	0.7	0.7	0.7
Ratio of specific heats $\gamma$	1.4	1.4	1.4	1.4
Gas constant $R$ [J/(kg·K)]	287	287	287	287
Domain length $L_x, L_y, L_z$	$12H, 30H, 6H$	$12H, 30H, 6H$	$12H, 30H, 6H$	$6H, 26H, 4H$
Grid number $N_x, N_y, N_z$	2200, 1400, 1100	2200, 1400, 1100	2200, 1400, 1100	2100, 2300, 1400

filtered value computed with a spatial average within a local and finite volume. The expression for  $\tau_\phi$  is obtained by the SGS scalar variance equation. It has been confirmed that the MVM works very well in Lagrangian particle simulation combined with the LES for incompressible flows [8].

In the present study, we consider the extension of the MVM to compressible turbulence, where density, viscosity, and diffusivity coefficient depend on space and time. We perform direct numerical simulation (DNS) of compressible planar jet with passive scalar transfer. *A-priori* test is performed for the MVM of molecular diffusion and thermal conduction.

## 2 DNS of Compressible Planar Jet

Direct numerical simulations are performed for temporally evolving compressible planar jet with a passive scalar transfer. Initial pressure is uniform in the computational domain and is  $P_a = 1.013 \times 10^5$  Pa. The initial velocity and scalar profiles are produced with the hyperbolic tangent profile [9] and velocity fluctuations generated by a diffusion process [10], where the jet core region has the streamwise velocity  $U_J$  and scalar  $\phi_J$ , while the initial jet width is  $H$ . Temperature of the jet core region and ambient fluids is 300K. At the edge of the jet, the temperature profile follows the Crocco-Busemann relation. The viscosity is given by Sutherland’s law. An initial density profile is obtained from the equation of state of ideal gas.

DNS is performed with the three-dimensional rectangular computational domain. The streamwise, lateral, and spanwise directions are represented by  $x$ ,  $y$ , and  $z$ , respectively. The jet center is given by  $y = 0$ . There are periodic boundaries in the  $x$  and  $z$  directions and the subsonic non-reflecting outflow boundary conditions [9] are applied in  $y$  direction. The grid spacing is uniform in the  $x$  and  $z$  directions, whereas the grid is stretched in the  $y$  direction near the lateral boundaries. The governing equations are three-dimensional Navier-Stokes equations for a compressible fluid and a transport equation for a passive scalar. The time advancement of Euler terms is computed by an explicit five-step fourth-order Runge-Kutta scheme [11], while the other terms arising from the viscous effects, molecular diffusion, and heat conduction are handled with an explicit first-order Euler scheme. Spatial derivatives are computed with the 8th-order explicit finite difference scheme [12] in interior domain, while the region near the boundaries is treated with an internal-biased lower-order scheme to maintain numerical stability except for the periodic boundaries [13].

The parameters in the DNS are summarized in Tab. 1. As reference quantities for nondimensionalizing the governing equations, we utilize  $H$  for the length,  $U_J$  for the velocity,  $\phi_J$  for the passive scalar, and  $H/U_J$  for the time. The Reynolds number and the Mach number of the planar jet are defined as  $Re_J = \rho_J U_J H / \mu_J$  and  $M_J = U_J / c_J$ , respectively, where  $\rho_J = P_a / RT_J$ ,  $\mu_J$  and  $c_J = \sqrt{\gamma RT_J}$  are the density, viscosity, and local speed of sound on the jet center ( $T_J$ : temperature on the jet center).

Passive scalar and temperature are visualized in Figs. 1 and 2, respectively. It can be found from  $\phi$  values near the centerline that the jet spreads more for lower  $M_J$ . It is also clear that the scalar field in Fig. 1(d) contains smaller-scale structures than in Figs. 1(a), (b), and (c) because of higher  $Re_J$ . In Fig. 2, temperature in the jet has increased from the initial value  $T_J$ , and the temperature is higher for higher  $M_J$ .

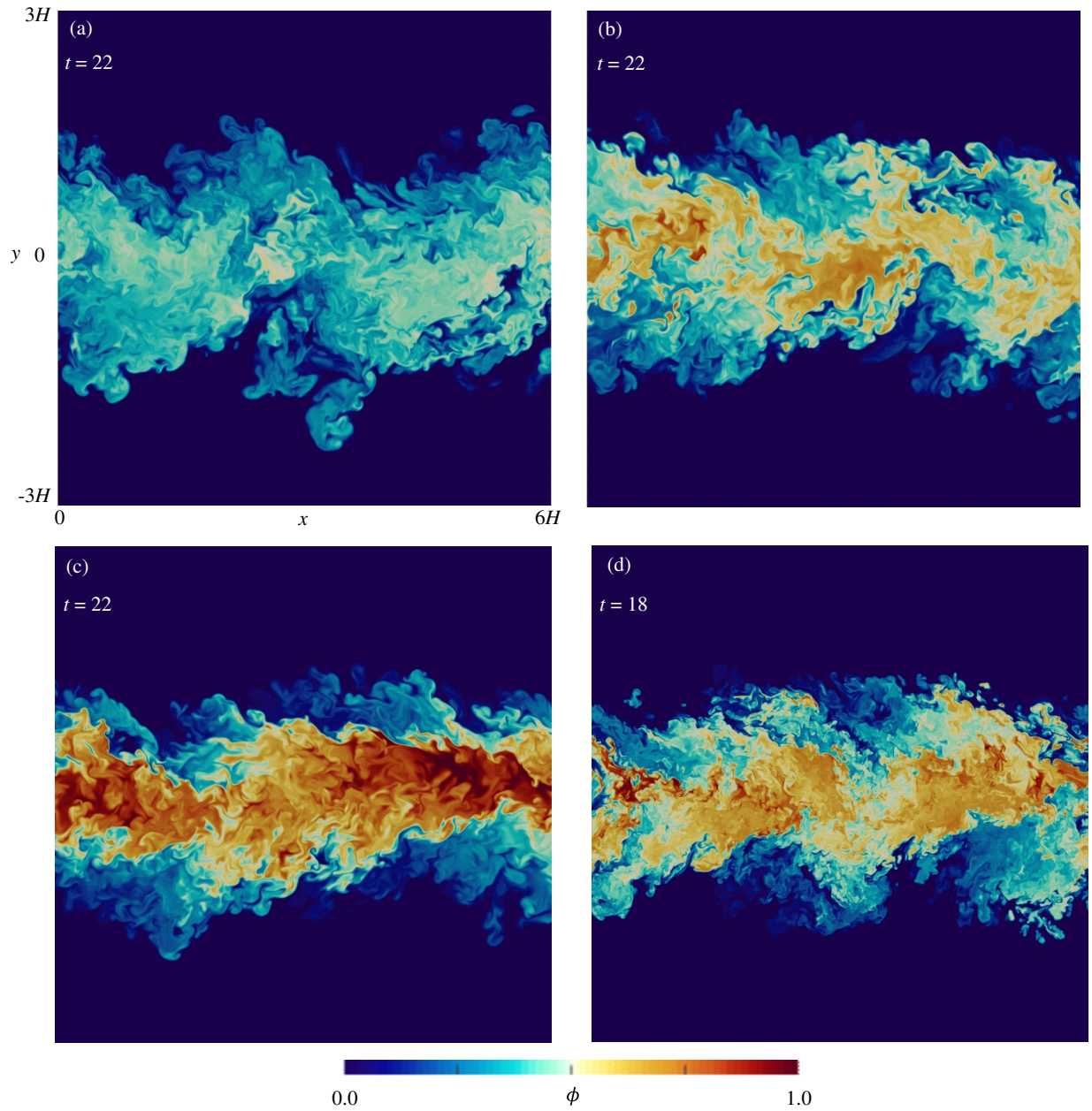


Figure 1: Visualization of the passive scalar field for (a) Run A ( $t = 22$ ), (b) Run B ( $t = 22$ ), (c) Run C ( $t = 22$ ), and (d) Run D ( $t = 18$ ) at  $z = 0$ .

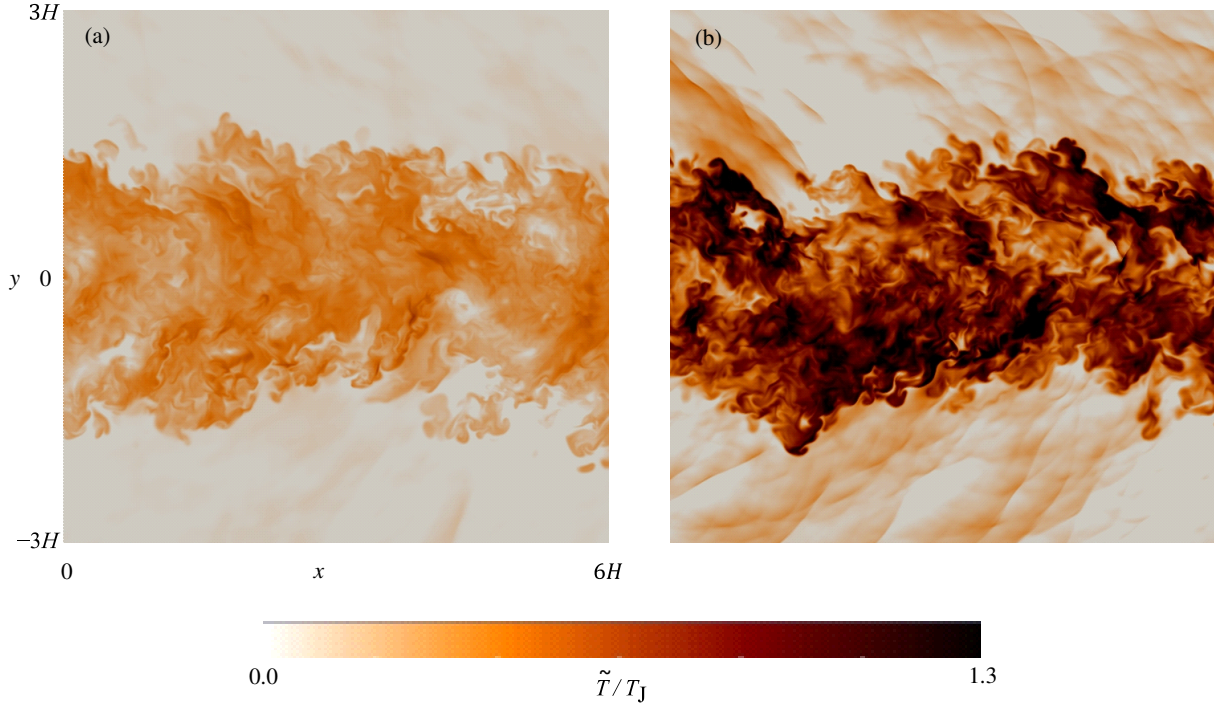


Figure 2: Visualization of the temperature field for (a) Run B ( $t = 22$ ) and (b) Run C ( $t = 22$ ) at  $z = 0$ .

### 3 *A-Priori* Test of MVM

The MVM has been developed for Lagrangian particle simulation (LP simulation) of turbulent mixing. The LP simulation is performed with notional particles, whose velocity is often obtained from LES. Equations that describe the temporal evolution of passive scalar  $\phi^{(n)}$  and temperature  $T^{(n)}$  of particle  $n$  have a molecular diffusion term  $D_\phi = \nabla \cdot (\rho D \nabla \phi)$  and a heat conduction term  $D_T = \nabla \cdot (k \nabla T)$ , where  $\rho$  is fluid density,  $D$  is diffusivity coefficient, and  $k$  is thermal conductivity. For modeling these effects on particle  $n$ , the MVM uses an interaction among particles within a finite local volume  $V$ .  $\langle f|V \rangle$  is defined as an ensemble average of particles within the volume  $V$ .  $D_\phi^{(n)}$ , and  $D_T^{(n)}$  are modeled by a relaxation process toward the average within a volume as below.

$$[D_\phi]_{\text{mix}}^{(n)} = \frac{1}{\tau_\phi} \left( \langle \phi|V \rangle - \phi^{(n)} \right); [D_T]_{\text{mix}}^{(n)} = \frac{1}{\tau_T} \left( \langle T|V \rangle - T^{(n)} \right), \quad (1)$$

where the subscript mix denotes the mixing model. The mixing timescales  $\tau_\phi$  and  $\tau_T$  are obtained from the transport equations for the SGS variance of passive scalar and temperature as follows

$$\tau_\phi = \frac{\langle \phi''^2|V \rangle}{\langle \varepsilon_\phi|V \rangle}; \tau_T = \frac{\langle T''^2|V \rangle}{\langle \varepsilon_T|V \rangle}. \quad (2)$$

These mixing timescales cause the variance within the mixing volume  $\langle f''^2|V \rangle = \langle f^2|V \rangle - \langle f|V \rangle^2$  to decay at the rate given by the passive scalar dissipation rate  $\langle \varepsilon_\phi|V \rangle$  ( $\varepsilon_\phi = D \nabla \phi \cdot \nabla \phi$ ) and temperature dissipation rate  $\langle \varepsilon_T|V \rangle$  ( $\varepsilon_T = k / \rho \nabla \phi \cdot \nabla \phi$ ) respectively.

DNS data of fully developed turbulent jet is used in *a-priori* test of MVM in compressible turbulence. As shown in Fig. 3, *a-priori* test of the MVM is carried out for a wide range of the number of particles  $N_m$  and radius  $r_m$  for mixing volume. A spherical mixing volume is assigned to each DNS grid point on the jet centerline. One particle (red) is placed at the center of the sphere, while other particles' (blue) positions are randomly determined within the volume. The variables ( $\rho^{(n)}$ ,  $k^{(n)}$ ,  $D^{(n)}$ ,  $\phi^{(n)}$ ,  $T^{(n)}$ ,  $\nabla \phi^{(n)}$  and  $\nabla T^{(n)}$ )

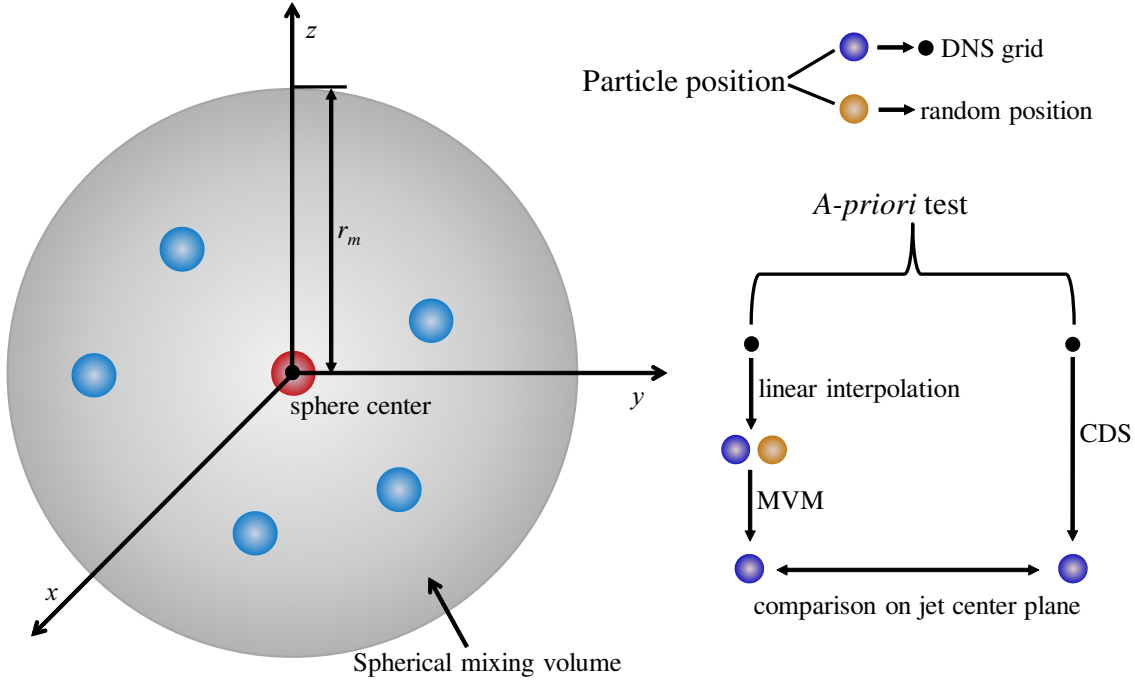


Figure 3: Schematic of *a-priori* test.

at the particle positions are obtained with a tri-linear interpolation of DNS data.  $[D_\phi]_{\text{mix}}$  and  $[D_T]_{\text{mix}}$  for the particle at the center are computed with the MVM as Eq. (1). These terms are also directly computed with the 8th-order central difference scheme (CDS), and they are denoted by  $[D_\phi]_{\text{CDS}}$  and  $[D_T]_{\text{CDS}}$ , which are directly computed with the 8th-order central difference scheme (CDS).

## 4 Results

For comparison between the MVM and CDS, correlation coefficient is introduced as below:

$$\text{Correlation coefficient} = \frac{\langle [D_A]_{\text{CDS}}' [D_A]_{\text{mix}}' \rangle}{\sqrt{\langle ([D_A]_{\text{CDS}}')^2 \rangle \langle ([D_A]_{\text{mix}}')^2 \rangle}}, \quad (3)$$

where  $f' = f - \langle f \rangle$  denotes the fluctuation from the mean value on the jet center plane, and  $A = \phi$  or  $T$ . Figure 4 shows the correlation coefficient for  $D_\phi$  [Figs. 4(a,b)] and  $D_T$  [Figs. 4(c,d)] as a function of  $(N_m, r_m)$  where  $r_m$  is normalized by the Kolmogorov length scale  $\eta$ . The magnitude of the correlation coefficient presented by color contours is almost the same as the one obtained in incompressible planar jets [14]. Higher values of correlation coefficients can be reached with an increase in  $N_m$  and a decrease in  $r_m/\eta$ , that is, an increase in particle density within a mixing volume. However, the dependence of the MVM performance on the Mach number is clear especially when  $N_m$  is large ( $N_m \geq 15$ ), where the correlation coefficient slightly decreases with the Mach number. The correlation coefficient for  $D_T$  [Figs. 4(c,d)] is similar to that for molecular diffusion [Figs. 4(a,b)].

A contribution to mean values of molecular diffusion and heat conduction can be examined with the conditional average of  $D_A$  on  $A$ , denoted by  $\langle D_A | A \rangle$ . The conventional average  $\langle D_A \rangle$  is related to  $\langle D_A | A \rangle$  with the pdf of  $A$ ,  $p(A)$ , as  $\langle D_A \rangle = \int p(A) \langle D_A | A \rangle dA$ .  $p(A) \langle D_A | A \rangle$  is plotted against the fluctuation  $A' = A - \langle A \rangle$  in Fig. 5. The results of CDS show that both molecular diffusion and heat conduction have a positive value for  $A' < 0$  and a negative value for  $A' > 0$  so that passive scalar and temperature approach the mean value  $\langle A \rangle$ . Under various conditions, the MVM well predicts  $p(A) \langle D_A | A \rangle$ . However, it is also

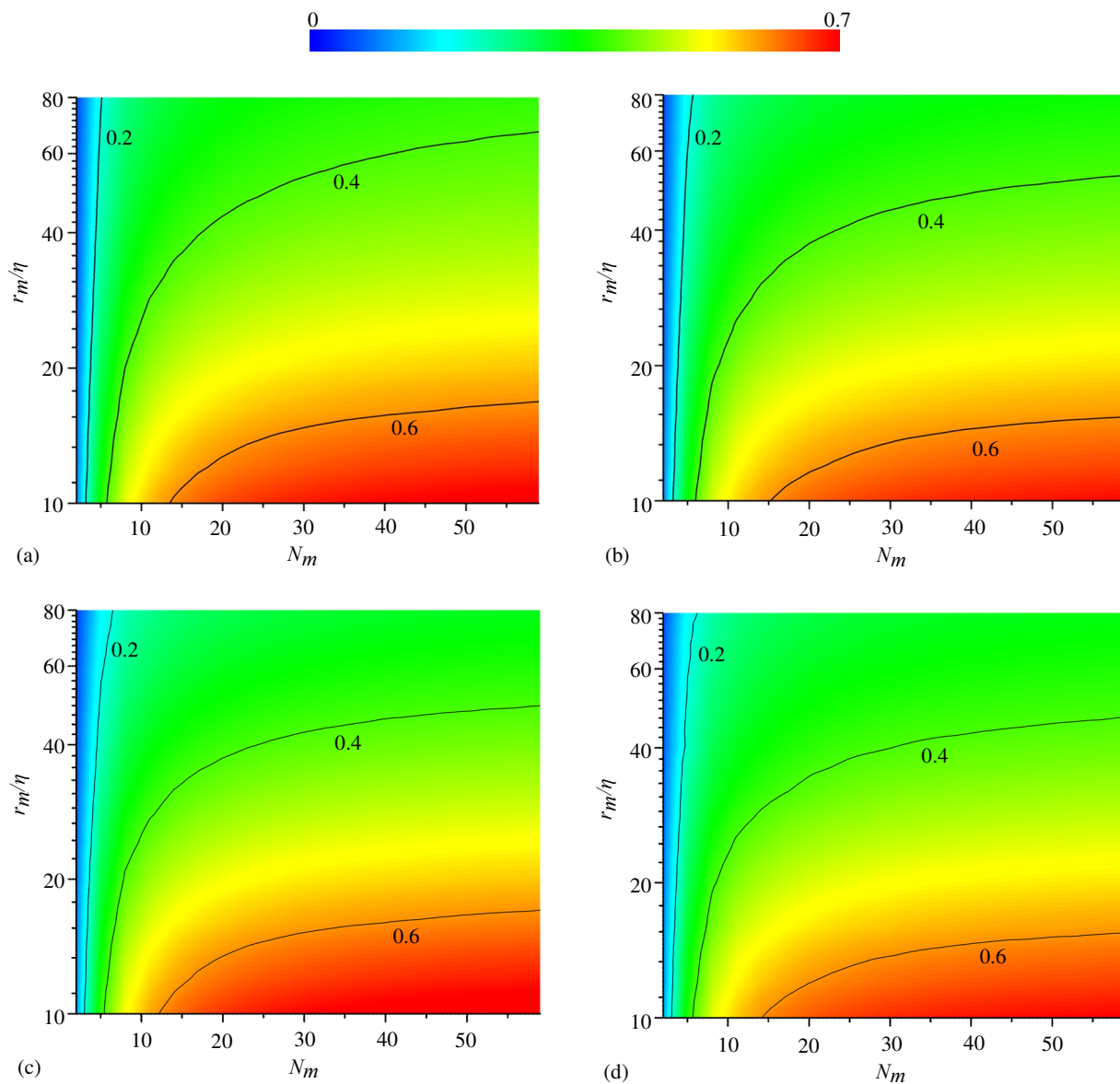


Figure 4: Correlation coefficient between  $[D_\phi]_{\text{mix}}$  and  $[D_\phi]_{\text{CDS}}$  as a function of  $(N_m, r_m)$  in (a) Run B and (b) Run C. Correlation coefficient between  $[D_T]_{\text{mix}}$  and  $[D_T]_{\text{CDS}}$  as a function of  $(N_m, r_m)$  in (c) Run B and (d) Run C. Solid lines are isolines of correlation coefficient equal to 0.2, 0.4, and 0.6.

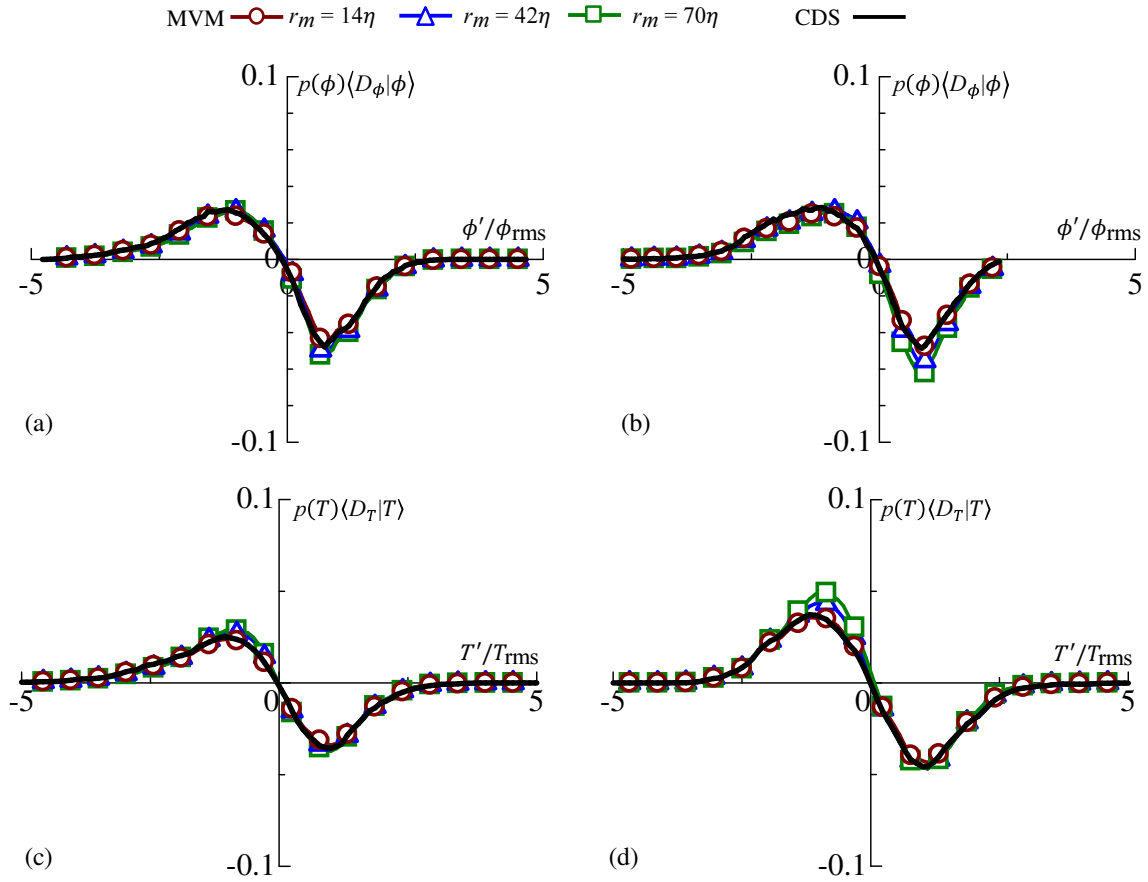


Figure 5: Molecular diffusion density,  $p(\phi)\langle[D_\phi]_{\text{CDS}}|\phi\rangle$  and  $p(\phi)\langle[D_\phi]_{\text{mix}}|\phi\rangle$ , in (a) Run B and (b) Run C; thermal conduction density,  $p(T)\langle[D_T]_{\text{CDS}}|T\rangle$  and  $p(T)\langle[D_T]_{\text{mix}}|T\rangle$ , in (c) Run B and (d) Run C. The plots are shown for  $r_m = 14\eta$ ,  $r_m = 42\eta$ , and  $r_m = 70\eta$  with  $N_m = 14$ .

found that the agreement between the CDS and the MVM is slightly degraded for  $0.5 < \phi'/\phi_{\text{rms}} < 1.5$  and  $-1.4 < T'/T_{\text{rms}} < -0.35$  at  $M_J = 2.6$ , though the MVM gives a closer value to the CDS for smaller mixing volume for higher Mach number cases. Figure 6 visualizes  $\varepsilon_\phi/\langle\varepsilon_\phi\rangle$  and  $\varepsilon_T/\langle\varepsilon_T\rangle$  and isolines of  $\phi'/\phi_{\text{rms}}$  for  $0.5 < \phi'/\phi_{\text{rms}} < 1.5$  and  $T'/T_{\text{rms}}$  for  $-1.4 < T'/T_{\text{rms}} < -0.35$ . We can find that the concentrated isolines appear on ramp-cliff structures with a high dissipation rate shown with black color. It is known that an increase in the Mach number makes intermittency in a scalar field stronger, which leads to the dramatic change in spatial profile of scalar dissipation rate [15]. A large mixing volume such as  $r_m = 70\eta$  cannot precisely capture these small-scale structures. Therefore, the MVM accuracy with a large mixing volume is slightly degraded especially in the case of  $0.5 < \phi'/\phi_{\text{rms}} < 1.5$  and  $-1.4 < T'/T_{\text{rms}} < -0.35$  in the compressible jets.

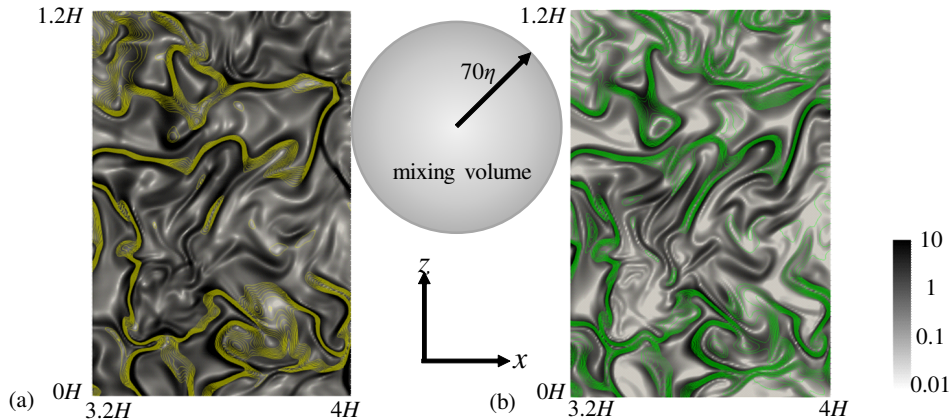


Figure 6: Visualization of (a) passive scalar dissipation rate and (b) temperature dissipation rate in Run C with log scale. Isolines are shown for  $\phi'/\phi_{\text{rms}}$  and  $T'/T_{\text{rms}}$  in the range of  $0.5 \leq \phi'/\phi_{\text{rms}} \leq 1.5$  and  $-1.4 \leq T'/T_{\text{rms}} \leq -0.35$ .

## 5 Conclusion

The mixing volume model (MVM) for compressible turbulence, based on the interaction among multiple particles within a finite local mixing volume, is developed for modeling molecular diffusion and heat conduction in compressible turbulence.

DNS is carried out for the three-dimensional compressible planar jet. Interpolating DNS data onto the position of notional particles, we perform *a-priori* test of the MVM for molecular diffusion term and heat conduction term, where the values obtained by the MVM are compared with those by the finite difference approximation. The MVM gives these terms positively correlated with the finite difference values. The degree of the correlation between the MVM and finite difference is dependent on the particle density within a mixing volume, and is slightly degraded at high Mach number, Because of strong intermittency in a scalar field arising at  $M_J = 2.6$ , the MVM with smaller mixing volume is suitable especially for higher Mach numbers.

## Acknowledgments

The numerical simulations presented in this manuscript were carried out on the high performance computing system in Nagoya University and the high performance computing system (NEC SX-ACE) in the Japan Agency for Marine-Earth Science and Technology. This work was partially supported by ‘‘Collaborative Research Project on Computer Science with High-Performance Computing in Nagoya University’’ and by MEXT KAKENHI Grant Numbers 18K13682 and 18H01367.

## References

- [1] Z. Pan, W. Cui, and Q. Miao. Numerical simulation of vortex-induced vibration of a circular cylinder at low mass-damping using RANS code. *Journal of Fluids and Structures*, 23(1):23–37, 2007.
- [2] J. W. Deardorff. A numerical study of three-dimensional turbulent channel flow at large Reynolds numbers. *J. Fluid Mech.*, 41(2):453–480, 1970.
- [3] H. G. Weller, G. Tabor, A. D. Gosman, and C. Fureby. Application of a flame-wrinkling LES combustion model to a turbulent mixing layer. In *Twenty-seventh Symposium (International) on Combustion*, pages 899–907. The Combustion Institute, Pittsburgh, 1998.
- [4] P. E. DesJardin and S. H. Frankel. Large eddy simulation of a nonpremixed reacting jet: Application and assessment of subgrid-scale combustion models. *Phys. Fluids*, 10(9):2298–2314, 1998.
- [5] A. Y. Klimenko. On simulating scalar transport by mixing between Lagrangian particles. *Phys. Fluids*, 19(3):031702, 2007.
- [6] A. Y. Klimenko. Lagrangian particles with mixing. II. Sparse-Lagrangian methods in application for turbulent reacting flows. *Phys. Fluids*, 21(6):065102, 2009.
- [7] R. O. Fox and A. Varma. *Computational models for turbulent reacting flows*. Cambridge Univ. Press, 2003.
- [8] T. Watanabe, Y. Sakai, K. Nagata, Y. Ito, and T. Hayase. LES–Lagrangian particle method for turbulent reactive flows based on the approximate deconvolution model and mixing model. *J. Comput. Phys.*, 294:127–148, 2015.
- [9] Z. Wang, J. Zhou, J. Fan, and K. Cen. Direct numerical simulation of ozone injection technology for NOx control in flue gas. *Energ. Fuel.*, 20(6):2432–2438, 2006.
- [10] A. Kempf, M. Klein, and J. Janicka. Efficient generation of initial-and inflow-conditions for transient turbulent flows in arbitrary geometries. *Flow Turbul. Combust.*, 74(1):67–84, 2005.
- [11] G. Lodato, P. Domingo, and L. Vervisch. Three-dimensional boundary conditions for direct and large-eddy simulation of compressible viscous flows. *J. Comput. Phys.*, 227(10):5105–5143, 2008.
- [12] C. A. Kennedy and M. H. Carpenter. Several new numerical methods for compressible shear-layer simulations. *Appl. Numer. Math.*, 14(4):397–433, 1994.
- [13] Z. Wang, P. He, Y. Lv, J. Zhou, J. Fan, and K. Cen. Direct numerical simulation of subsonic round turbulent jet. *Flow Turbul. Combust.*, 84(4):669–686, 2010.
- [14] T. Watanabe and K. Nagata. Mixing model with multi-particle interactions for Lagrangian simulations of turbulent mixing. *Phys. Fluids*, 28(8):085103, 2016.
- [15] Q. Ni. Compressible turbulent mixing: Effects of compressibility. *Phys. Rev. E*, 93(4):043116, 2016.